Celest Mech Dyn Astr (2009) 103:191–207
DOI 10.1007/s10569-008-9175-0

ORIGINAL ARTICLE

The rectilinear three-body problem using symbol sequence II: role of the periodic orbits

Masaya Masayoshi Saito · Kiyotaka Tanikawa

Received: 11 May 2007 / Revised: 25 August 2008 / Accepted: 15 November 2008 /
Published online: 30 January 2009

Abstract We study the change of phase space structure of the rectilinear three-body problem when the mass combination is changed. Generally, periodic orbits bifurcate from the stable Schubart periodic orbit and move radially outward. Among these periodic orbits there are *dominant* periodic orbits having rotation number $(n-2)/n$ with $n \geq 3$. We find that the number of dominant periodic orbits is two when n is odd and four when n is even. Dominant periodic orbits have large stable regions in and out of the stability region of the Schubart orbit (Schubart region), and so they determine the size of the Schubart region and influence the structure of the Poincaré section out of the Schubart region. Indeed, with the movement of the dominant periodic orbits, part of complicated structure of the Poincaré section follows these orbits. We find stable periodic orbits which do not bifurcate from the Schubart orbit.

Keywords Three-body problem · Chaos · Symbolic dynamics · Periodic orbit

1 Introduction

In the present study, we continue our work on the rectilinear three-body problem (Saito and Tanikawa 2007; hereafter referred to as Paper I). The rectilinear three-body system is such that three particles are on a line. This problem has two degrees of freedom.

The structure on the surface of section of the rectilinear three-body system has been studied using the Poincaré map (Hietarinta and Mikkola 1993; hereafter HM1993). They found that the Poincaré section is divided into three basic regions: the Schubart region, the chaotic scattering region, and the immediate escape region. Inside the scattering region, the interplay time is so sensitive to the initial conditions that there seemed to be no structure. HM1993 also

M. M. Saito (✉)
The Institute of Statistical Mathematics, 4-6-7 Minami-Azabu, Minato-ku, Tokyo 106-8569, Japan
e-mail: sasame2005@mail.goo.ne.jp

K. Tanikawa
National Astronomical Observatory of Japan, Osawa 2-21-1, Mitaka, Tokyo 181-8588, Japan
e-mail: tanikawa.ky@nao.ac.jp

found that, the number of scallops, which constitute the immediate escape region, increases as the mass of the central particle becomes smaller.

Tanikawa and Mikkola studied the structure of the Poincaré section for the equal-mass case using symbol sequences which record the collisional history of orbits (Tanikawa and Mikkola 2000a). They used the Poincaré section as the initial condition surface and associated with each point of the surface its future history including the final motion. They then succeeded in showing that the chaotic scattering region is filled with points whose orbits end with triple collision and that these points form well stratified curves. This uncovered structure in the chaotic scattering region shows that (1) stratified triple collision curves make a *sector* together with the sub-region of the immediate escape region (i.e., scallop); (2) four sectors surround the Schubart region. Tanikawa and Mikkola further studied the distribution of symbol sequences in the equal-mass case (Tanikawa and Mikkola 2000b); they found unallowable words and built a transition graph among local regions in the Poincaré section.

The study of a similar dynamical system, the collinear Coulomb three-body problem with electron-ion-electron configuration, carried out by Sano (2004) is helpful to understand our system. In his system, there exist the Schubart region and unstable periodic points on its vertices. He confirmed the existence of the separatrices of these unstable points in his system numerically following the mapped points starting near the vertices.

In Paper I, we studied how the structure on the Poincaré section changes as the central mass varies. A schematic illustration for components of the structure is displayed in Fig. 1 (a reproduction of Fig. 2 in Paper I). The chaotic scattering region is foliated with triple collision curves in general mass configurations. This foliation makes three types of blocks: (VI) *arches*, (VII) *germs*, and (VIII) *pipelines*. Arches and germs are distinguished by whether two terminal points of a triple collision curve are the same or not: different in an arch and the same in a germ. These terminal points are located on the horizontal axis and called (X) *foot-points*. Throughout the present paper, we say sometime 'the symbol sequence of p is s,' if an orbit starting from p on the Poincaré section produces symbol sequence s. In Paper I, we

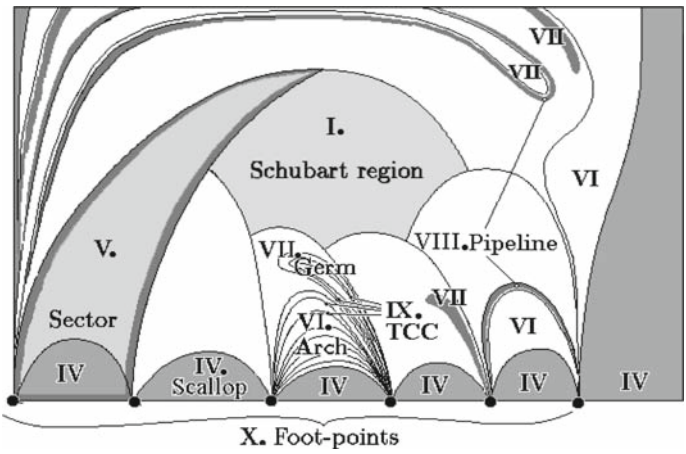

Fig. 1 The schematic illustration of the structure on the Poincaré section. The Poincaré section consists of the Schubart region (I) and sectors (V). A sector (V) includes one scallop (IV), one arch (VI), optional germs (VII) and pipelines (VIII). In the third sector from the left, it is shown that both an arch and a germ consist of the strata of triple collision curves. In the blank area of the third sector, there are other germs and/or pipelines, although they are not drawn. The pipeline (VIII) is an object which connects two germs in different sectors. Note that there are narrow escape regions also inside the sectors

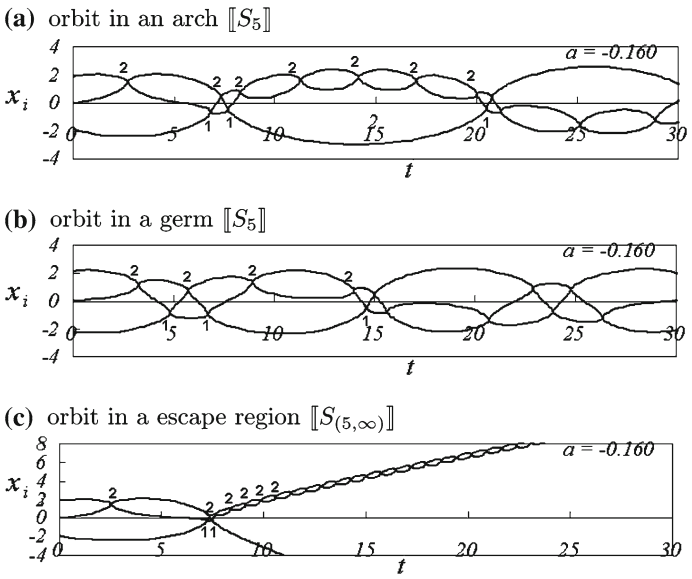

Fig. 2 Orbit description at $a = -0.160$ for initial points in (**a**) a branch of $[\![S_5]\!]$ in an arch, (**b**) $[\![S_5]\!]$ in a germ, and (**c**) $[\![S_{(5,\infty)}]\!]$ in a scallop. Symbols for collisions are also printed

introduced sets of symbol sequences and partitioned the Poincaré section in regions so that all points in a region have certain symbol sequences of similar characters. This partitioning revealed a continuity between the (I) *Schubart region* and the (III) *chaotic scattering region* in the following sense that the orbits with initial values in the Schubart region repeat alternate collision of the central particle with the left and right particles infinitely, whereas those in the chaotic scattering region repeat finitely. It should be noted that there is a narrow escape region between any two neighbouring strata in an arch. According to numerical results of Orlov et al. (2008), the interplay time is almost the same inside each of these escape regions, whereas it is longer as an escape region is located nearer to the Schubart region.

Paper I numerically showed that, the chaotic scattering region consists only of arches at the totally degenerated cases, at least in the resolution of the initial value space. When the central mass varies, at every passage of totally degenerated case, not only the number of arches increases but also regions in arches are replaced. We found, through the observation for the intermediate mass ratio, that germs first appear as a branch of arches and then construct or re-construct arches. Pipelines play a role connecting branches of a region, when these branches exist in different germs. A dynamical explanation of these germs' behaviour was left as an open question.

In the present paper, we continue to study the structure change of the Poincaré section as the central mass varies (we only consider the symmetric mass combinations). However, in contrast to Paper I, the structure is analysed in relation to the motion of periodic orbits bifurcated from the Schubart orbit. From another point of view, the azimuthal structure of the Poincaré section with center at the Schubart point has been studied in Paper I, whereas the radial structure with center at the Schubart point is studied in the present paper. The Schubart orbits appears as the fixed point in the Poincaré section. A rotation number around this fixed point shall be introduced in order to analyse a general tendency of the motion of the bifurcated orbits from the fixed point. As we shall see, there is the sequence of rotation numbers such that the corresponding periodic orbits has significant influence on the

Poincaré section. We mainly concern with these orbits. As the mass parameters change, such periodic orbits bifurcate, recede from the fixed point, and their stability region shrink. We shall relate these behaviours of periodic points to the growth of the germs observed in Paper I.

The organization of the present paper is the following: In Sect. 2, we introduce the equations of motion of our system. We define the Poincaré section and introduce the *rotation number* in the fixed-point-centric coordinates. The Sect. 3 is for the results. In Sect. 3.1, the bifurcation of periodic points is analysed as the mass parameter changes. In Sect. 3.2, we find that periodic points with special rotation number are dominant over the structure of the Poincaré section. In Sect. 3.3, we show in detail the radial motion of the periodic point with the growth of the germs as the mass parameter changes. Finally in Sect. 4, we summarize our results.

2 Method

2.1 Equations of motion and initial points

Let m_1, m_0, and m_2 denote the masses of the three particles from left to right on the line. We restrict ourselves to symmetric mass configuration ($m_1 = m_2$), since we saw in Paper I that asymmetry of the mass configuration in many cases does not add topologically new structure to the symmetric case. Because of scaling invariance we can normalize the total mass to 3, and then parametrise three masses in a symmetric configuration as follows:

$$m_1 = m_2 = 1 - a \text{ and } m_0 = 1 + 2a, \text{ where } -1/2 < a < 1. \tag{1}$$

Let (q_1, q_2) be the distances $\overline{m_1 m_0}$ and $\overline{m_0 m_2}$, and (p_1, p_2) the conjugate momenta to (q_1, q_2). The Hamiltonian H is written as

$$\begin{aligned} H = &\left[\frac{1}{2}\left(\frac{1}{m_1}+\frac{1}{m_0}\right)p_1^2 + \frac{1}{2}\left(\frac{1}{m_0}+\frac{1}{m_2}\right)p_2^2 - \frac{p_1 p_2}{m_0}\right] \\ &-\left[\frac{m_1 m_0}{q_1} + \frac{m_0 m_2}{q_2} + \frac{m_1 m_2}{q_1+q_2}\right]. \end{aligned} \tag{2}$$

We consider the case $H = E < 0$, and further restrict ourselves to the case $E = -1$. The latter restriction is justified by the fact that negative energy system can be brought to $E = -1$ using the homogeneity of the force function (the second bracket in Eq. 2).

A Poincaré section $\overline{\Pi}$ is introduced as a two-dimensional surface where $q_1 = q_2$ holds. A point on this surface is specified by two parameters (R, θ). The first parameter $R \equiv (q_1 + q_2)/2$ is a scale parameter of the system. In negative E cases, R has the maximal value $R_{\max}$:

$$R_{\max} = \frac{1}{|E|}\left(m_0 m_1 + m_0 m_2 + \frac{1}{2} m_1 m_2\right). \tag{3}$$

A value of R determines the value of q_1 and q_2 because of the constraints coming from the definition of R and the Poincaré section. Therefore, R also determines the size of kinetic energy (the first bracket in Eq. 2). In order to determine $\dot{q}_1$ and $\dot{q}_2$, we add the second parameter θ. The concrete definition of θ is described in Mikkola and Hietarinta (1989) and Paper I. The domain of θ is $0 \leq \theta < 2\pi$ and there is the relation $\dot{\boldsymbol{q}}(\theta + \pi) = -\dot{\boldsymbol{q}}(\theta)$, where we denote by $\dot{\boldsymbol{q}}(\theta)$ the $(\dot{q}_1, \dot{q}_2)$ for given θ. We split the Poincaré section $\overline{\Pi}$ at $\theta = \pi$ and denote

the side with $\theta < \pi$ by Π and the side with $\theta \geq \pi$ by Π^*. As we did in Paper I, we only study the structure of the side Π for the future integration. If one wants to exhaust the phase space by only the integration of orbits with initial values on the side Π, one should integrate the orbits for the future and the past. The reason why our non-exhaustive approach is justified is that orbits in the chaotic scattering region, which is the target of interest, intersect with Π and Π^* multiple times.

There are three types of collision in our system: left-center ($q_1 = 0, q_2 \neq 0$), center-right ($q_2 = 0, q_1 \neq 0$), and triple ($q_1 = q_2 = 0$) collisions. Let us denote these collisions by symbols '1', '2', and '0', respectively. We study the evolution of orbits using the symbol sequences instead of orbits themselves. It is to be noted that, we encode into symbol sequences the future behaviour of the orbits starting at points of the Poincaré section. Therefore symbol sequences are not bi-infinite but singly infinite to the future.

In our preliminary research (Saito and Tanikawa 2004), we introduced cylinders (sets of symbol sequences with given words where a word is a finite sequence of symbols) $S_{c,j}$, $S_{c,\infty}$ and S_c:

$$\begin{cases} S_{2i+1,j} \equiv \{(21)^i (2)^j w | w \text{ is an arbitrary infinite word}\} & \text{with } i \geq 0 \text{ and } 1 \leq j < \infty \\ S_{2ij} \equiv \{(21)^i (1)^j w | w \text{ is an arbitrary infinite word}\} & \text{with } i \geq 1 \text{ and } 1 \leq j < \infty \end{cases} \tag{4}$$

$$\begin{cases} S_{2i+1,\infty} \equiv \{(21)^i (2)^\infty\} & \text{with } i \geq 0 \\ S_{2i,\infty} \equiv \{(21)^i (1)^\infty\} & \text{with } i \geq 1 \end{cases} \tag{5}$$

$$S_c \equiv \bigcup_{j<\infty} S_{c,j}. \tag{6}$$

Let $[\![S]\!]$ denote the regions on Π such that each point on $[\![S]\!]$ has a symbol sequence in S. The three basic regions in HM1993 correspond to our regions as follows:

Immediate escape region	$[\![S_{(c,\infty)}]\!]$	$1 \leq c \leq n_{\mathrm{FOP}}$
Chaotic scattering region	$[\![S_c]\!] \cup [\![S_{(c',\infty)}]\!]$	$1 \leq c < \infty,\ n_{\mathrm{FOP}} + 1 \leq c' < \infty$
Schubart region	$[\![S_c]\!]$	$c = \infty$

We here show an example of orbits in Fig. 2 helpful to understand the meaning of the introduced cylinder sets. All panels show orbits at $a = -0.160$ and the whole Poincaré section for this a shall be displayed at Fig. 9b. Panels (a) and (b) are orbits taken from region $[\![S_5]\!]$ but the respective branches of the region belong to an arch in (a) and a germ in (b). In Fig. 9b, the numbers 5 and $5'$ are printed on these branches, respectively. These panels are an example showing that orbits with initial values on $[\![S_{2k+1}]\!]$ experiences $2k$ times alternate collisions like the Schubart orbit does (until $t < 8$ in both the panels), one-sided collisions between m_0 and m_2 (until $t < 20$ in the panel (a) or $t < 15$ in the panel (b)), and a pattern of collisions corresponding to the arbitrary word in $[\![S_{2k+1}]\!]$, whichever the initial values is on an arch or a germ. The change from alternate to one-sided collisions occurs at a triple approach, and in the panel (a) compared with the panel (b), more compact triple approach and more number of one-sided collision are experienced. If a sufficiently compact triple approach occurs, the number of one-sided collisions is infinite. This is the case shown in panel (c), which is an orbit with initial values at $[\![S_{(5,\infty)}]\!]$.

Integration of orbits are carried out for grid points. We introduce the grid points (θ_i, R_i) with different resolution on Π:

$$(\theta_i, R_i) = \left(\pi \times \frac{i}{\theta_{\rm div}}, R_{\max} \times \frac{j}{R_{\rm div}}\right), \text{ where } i = 0, \ldots, \theta_{\rm div} - 1,\ j = 1, \ldots, R_{\rm div}, \text{ and}$$
$$\text{(i) } \theta_{\rm div} = 540,\ R_{\rm div} = 300 \quad \text{or} \quad \text{(ii) } \theta_{\rm div} = 1,800,\ R_{\rm div} = 1,000. \tag{7}$$

Most of structures on the Poincaré section and their change due to the mass variation can be resolved with resolution (i). Detailed structures could be lost, if one used resolution (i). However, once we understand certain fine structures with resolution (ii), we can use resolution (i) to follow global behaviour of the structure of the Poincaré section when mass parameters are changed. We have obtained the first 64 digits of symbol sequences for the grid points through integration of orbits. These constitute the basic data in the rest of the paper for the distribution of symbol sequences on Π.

2.2 Poincaré map and rotation number

We here define the Poincaré map on the Poincaré section (θ, R). An orbit starting from the Poincaré section repeats the intersection with Π and Π^* alternately. When an orbit intersects with Π (resp. Π^*) at (θ, R) and Π (resp. Π^*) again at (θ'', R''), we define a map T from (θ, R) to (θ'', R'').

$$T : (\theta, R) \mapsto (\theta'', R''), \text{ where } (\theta, R), (\theta'', R'') \in \Pi \quad \text{or } (\theta, R), (\theta'', R'') \in \Pi^* \tag{8}$$

The equations of motion have a simple periodic solution, the so-called Schubart orbit (Schubart 1956), whose symbol sequence is $(21)^\infty$. The intersection $\boldsymbol{P}_0 = (\theta_0, R_0)$ of the Schubart orbit with Π is a fixed point of the map, namely $\boldsymbol{P}_0 = T(\boldsymbol{P}_0)$. The linear stability of T around $\boldsymbol{P}_0$ over the mass triangle is studied by HM1993. Approximately in the mass combinations such that $m_1 < m_0 < m_2$, $\boldsymbol{P}_0$ is hyperbolic whereas in the other combinations it is elliptic. The stability region is called the Schubart region. A point $\boldsymbol{P}$ such that $\boldsymbol{P} = T^q(\boldsymbol{P})$ is called a *q-periodic point* and the sequence $\{\boldsymbol{P}, T^1(\boldsymbol{P}), \ldots, T^{q-1}(\boldsymbol{P})\}$ is called a *q-periodic orbit*. We are interested in the periodic orbits that bifurcate from the fixed point as the mass parameter a is changed.

In order to describe the elliptic motion around $\boldsymbol{P}_0$, we introduce the *rotation number*. The rotation number is the averaged number of rotations per iterate of T. As for complete description of this quantity, see the text book by Contopouls (2002). First, we introduce polar coordinates (D, A) with center at $\boldsymbol{P}_0 = (\theta_0, R_0)$:

$$D\cos A = (\theta - \theta_0)\mathrm{g}_\theta, \quad D\sin A = (R - R_0)\mathrm{g}_R,$$

where $\mathrm{g}_\theta = 180/\pi$ and $\mathrm{g}_R = 100/R_{\max}$. The values of g_θ and g_R are arbitrarily chosen such that both θ and R equally contribute to the values of D and A. Now the Poincaré map is expressed as $T : (D, A) \mapsto (D', A')$. We then introduce the effective rotation number $\nu_n(D, A; a)$ and the (exact) rotation number $\nu_\infty(D, A; a)$ at $(D, A; a)$ in the following equations:

$$\mathrm{diff}(A', A) = \begin{cases} A' - A & (\text{if } A' - A \geq 0) \\ A' - A + 2\pi & (\text{if } A' - A < 0) \end{cases} \tag{9}$$

$$\nu_n((D, A); a) = \frac{1}{2n\pi} \sum_{i=1}^{n} \mathrm{diff}(A^{(i)}, A^{(i-1)}), \quad \text{where } (D^{(i)}, A^{(i)}) = T^i(D, A) \tag{10}$$

$$\nu_\infty((D, A); a) = \lim_{k\to\infty} \nu_k(D, A; a) \quad (\text{if the limit exists}). \tag{11}$$

We here remark several points related to the numerical calculation of the rotation number. The first point is the selection of n of the $\nu_n((D, A); a)$. In our approach, we first take an

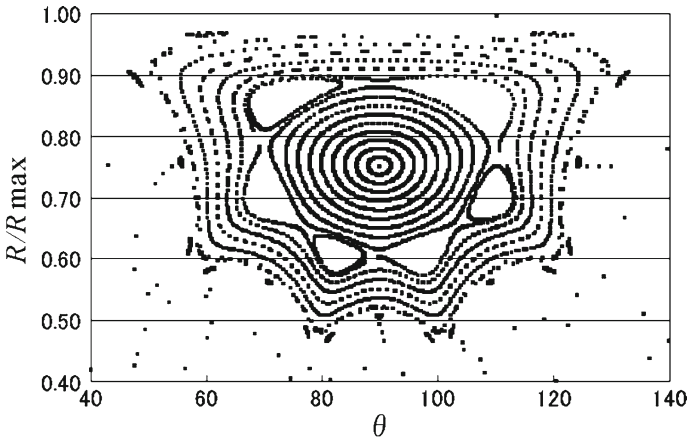

Fig. 3 A Poincaré map in order to select candidates for periodic points. In this map, $a = -0.25$ and the expected periodic points are those with $\nu = 4/6$. The centers of elliptic motions under the Poincaré map are the candidates

fixed integer N and iterate the mapping N times. We then find a number n ($1 \leq n \leq N$) such that $\mathrm{diff}(A^{(n)}, A) = \min_{1 \leq i \leq N}\{\mathrm{diff}(A^{(i)}, A)\}$. The second point concerns the rotation number of periodic points. Suppose p and q are integers. If $\boldsymbol{P}$ is a periodic point, then there exist integers p and q such that $\nu_q(\boldsymbol{P}; a) = \nu_\infty(\boldsymbol{P}; a) = p/q$ (by the above method of selection of n, $n = q$). This coincidence of the effective and exact rotation numbers helps us to find the periodic points: the points on the contour with $\nu_q(\boldsymbol{P}; a) = p/q$ on the the Poincaré section are the candidates of the periodic points with $\nu_\infty(\boldsymbol{P}; a)$. The third point is that the rotation number $\nu_\infty(\boldsymbol{P}_0; a)$ is calculated from the eigenvalues of linearized map of T at P_0. When this value is rational, the fixed point and the periodic points are degenerated. If the mass parameter a is changed, the periodic points bifurcate from fixed point $\boldsymbol{P}_0$.

2.3 Search for the periodic points

We explain how to detect the periodic points. First, we have to calculate $\lim_{D \to 0} \nu_\infty((D, A); a)$ for various values of a. For a given rotation number p/q, we can determine the mass parameter a where corresponding periodic points appear: solve $\nu_\infty(\boldsymbol{P}_0; a) = p/q$ for a. Second, we find candidates at a mass parameter a little distant from the exact bifurcation. The candidates for periodic points are found from the Poincaré map such as is shown in Fig. 3. The candidates for elliptic points can be taken at the center of the libration and for hyperbolic points at the saddle between two liberations.

Finally, we obtain a periodic point through the Newton–Raphson method (Eq. 12) starting from an arbitrary point on the contour. This method is used in Mikkola and Hietarinta (1991) to find the fixed point.

$$\mathbf{X}_{n+1} = \mathbf{X}_n - \left[\frac{\partial T(\mathbf{X}_n)}{\partial \mathbf{X}_n} - 1\right]^{-1} (T^p(\mathbf{X}_n) - \mathbf{X}_n) = 0. \tag{12}$$

Table 1 The values of a at which the periodic points bifurcate for several rotation numbers

ν_∞	1/4	1/3	2/4	3/5	4/6	3/7
a	0.61	0.41	−0.019	−0.15	−0.25	−0.31

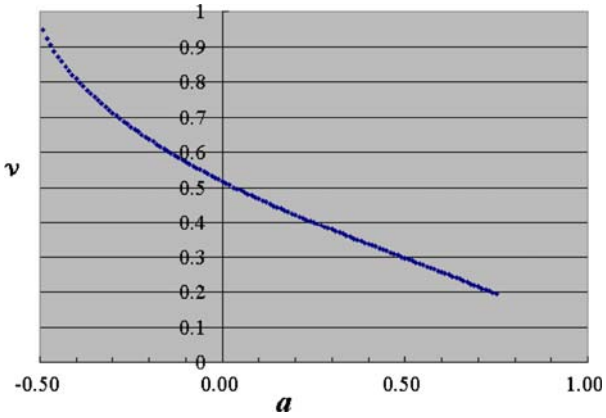

Fig. 4 The rotation number $\nu(\boldsymbol{P}_0, a)$ as a function of a

3 Results

We now show the behaviour and influence of the periodic points on the Poincaré section. First, their bifurcation and radial movement away from the Schubart orbit will be discussed. The values of parameter a where the periodic points bifurcate can be determined from the rotation number, $\nu_\infty(\boldsymbol{P}_0; a)$, of the Schubart orbit as a function of a. The relation between radial movement and the variation of a will be studied. Second, the number of orbits which appear in respective bifurcations for special rotation numbers will be discussed. Finally, the influence of such special periodic orbits on the Poincaré section will be discussed.

3.1 Bifurcation as the parameter changes

In this subsection, we show how periodic points bifurcate and move outward from the fixed point $\boldsymbol{P}_0$, when the parameter a is changed. As is stated in Sect. 2.2, period-q points bifurcate if $\nu_\infty(\boldsymbol{P}_0; a) = p/q$ with integers p and q. In order to know when the periodic orbits bifurcate, we calculate $\nu_\infty(\boldsymbol{P}_0; a)$ as a function of a (Fig. 4). For several rotation numbers, we show the values of a in Table 1. Figure 4 shows that $\nu_\infty(\boldsymbol{P}_0; a)$ is monotonic:

$$\frac{\partial \nu_\infty(\boldsymbol{P}_0; a)}{\partial a} < 0. \tag{13}$$

Therefore, for each rational number p/q, the periodic points with $\nu_\infty = p/q$ bifurcate once and for all. Note that, this graph shows that the period-3 orbit bifurcates at $a = a_{1/3} \fallingdotseq 0.41$. According to Moser (1958), generally in Hamiltonian systems when the period-3 orbit bifurcates, the mother periodic orbit becomes unstable. As an application of this result, he tried to explain the origin of the Kirkwood gaps. Also in our system, the instability at the bifurcation of the period-3 orbit was confirmed by Hietarinta and Mikkola (1993). We have followed the position of the periodic points with $\nu_\infty = 1/3$ on the Poincaré section with continuously changing a. As a result, when a is decreased, with a passage $a = a_{1/3}$, the triangle formed by these periodic points approaches ($a > a_{1/3}$), collides ($a = a_{1/3}$) with,

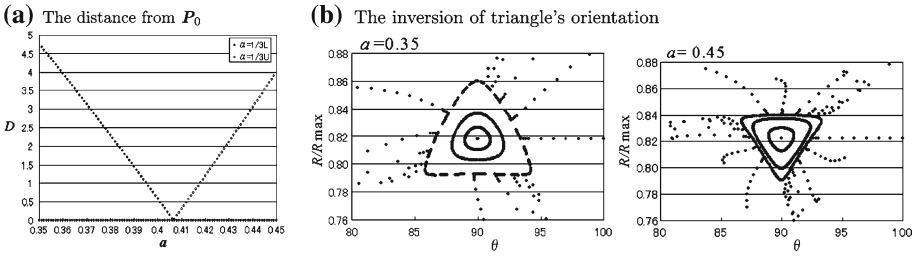

Fig. 5 The radial movement of the periodic points with $\nu_\infty = 1/3$ from $\boldsymbol{P}_0$. (**a**) the distance between one of these point and $\boldsymbol{P}_0$

and recedes ($a < a_{1/3}$) from $\boldsymbol{P}_0$ (Fig. 5a). The orientation of the triangle is inverted before and after $a_{1/3}$ (Fig. 5b). Similar behaviour was observed by Hénon (1970) in Hill's case of the restricted three-body problem. In his case, mother periodic orbit is the retrograde satellite orbit.

We want to know the direction of change of a for the bifurcated periodic points to move outward from $\boldsymbol{P}_0$. Suppose that the periodic points bifurcate at $a = a_{p/q}$ and exist at $a = a_{p/q} + da$ as the points with a finite distance dD from $\boldsymbol{P}_0$. The sign of da can be obtained from Eqs. 13 and 15, as follows. The total differential of ν as a function of a and D at $\boldsymbol{P}_0$ is

$$d\nu = \left(\frac{\partial \nu}{\partial a}\right)\Big|_{\boldsymbol{P}_0} da + \left(\frac{\partial \nu}{\partial D}\right)\Big|_{\boldsymbol{P}_0} dD.$$

Since $d\nu = 0$ on periodic points, we obtain

$$da = -\left(\frac{\partial \nu}{\partial D} \Big/ \frac{\partial \nu}{\partial a}\right)\Big|_{\boldsymbol{P}_0} dD\ . \tag{14}$$

We only need the sign of $\partial \nu_\infty(\boldsymbol{P}_0; a)/\partial D$, since we already know the sign of $\partial \nu_\infty(\boldsymbol{P}_0; a)/\partial a$. We approximate the derivative $\partial \nu_n(\boldsymbol{P}; a)/\partial D$ by the difference $(\nu_n((D + \Delta D, A); a) - \nu_n((D, A); a))/\Delta D$ for small ΔD. Since $\partial \nu_n(\boldsymbol{P}_0; a)/\partial D$ should be independent to A, we select arbitrarily the value of A: $A = 0$. Moreover, we have $\nu_\infty(\boldsymbol{P}_0; a) \fallingdotseq \nu_n(\boldsymbol{P}_0; a)$ for large $n \leq N$: $N = 256$. Finally we put $\Delta D = 0.1$. Figure 6

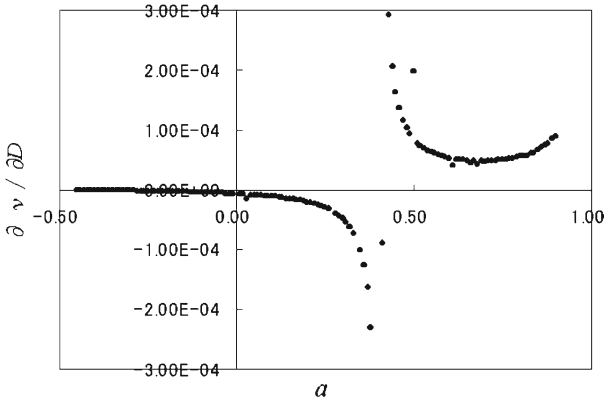

Fig. 6 Dependence of $\partial \nu(D, a)/\partial D$ on a. The sign of $\partial \nu(D, a)/\partial D$ changes at $a = a_{1/3}$

shows $\partial \nu_\infty(\boldsymbol{P}_0; a)/\partial D$ as a function of mass parameter a. The figure shows that the sign of $\partial \nu_\infty(\boldsymbol{P}_0; a)/\partial D$ is

$$\begin{cases} \frac{\partial \nu_\infty(\boldsymbol{P}_0;a)}{\partial D} > 0 & (\text{for } a > a_{1/3}) \\ \frac{\partial \nu_\infty(\boldsymbol{P}_0;a)}{\partial D} < 0 & (\text{for } a < a_{1/3}) \end{cases} \tag{15}$$

Taking into account Eqs. 13 and 15, and $dD > 0$, we find that da is positive for $a > a_{1/3}$ and negative for $a < a_{1/3}$. The recession from $a = a_{1/3}$, irrespective of the sign of a, yields successive recessions of the periodic points from the Schubart orbit. This implies that absence of the periodic points at $a = a_{1/3}$ (except for the periodic points independent of $\boldsymbol{P}_0$).

3.2 Dominant periodic orbits

In the present subsection, we will find periodic orbits and follow their motions for various rotation number. These results show us that the periodic orbits with rotation number $(n-2)/n$ dominate the structure of the Poincaré section. We call these the *dominant periodic orbits*. We discuss a few features of the dominant periodic orbits. On the other hand, periodic orbits with the other rotation numbers have too small stable regions to numerically find the location on the Poincaré section, so we do not consider these.

According to our numerical results, there is a rule for the number of dominant periodic orbits. number of these orbits is $\nu_\infty = (n-2)/n$. Indeed, for even n, the period is not n but $n/2$, and therefore, if we would strictly write the rotation number, it should be $\nu_\infty = (n/2-1)/(n/2)$. We have found the following rule for the number of periodic points.

A Rule *For the number of dominant periodic orbits with $\nu_\infty = (n-2)/n$, the following rule is confirmed from $n = 4$ to $n = 19$.*

- *the number of orbits is two for odd n.*
- *the number of orbits is four for even n.*

We show an example of this rule in Fig. 7 ($n = 5$ and 6) and Fig. 8 ($n = 17$ and 18). For the case of $n = 3$ ($\nu_\infty = 1/3$), only one unstable orbit appears through bifurcation as already seen in Fig. 5b. It is important to note that according to the Poincaré–Birkhoff theorem (Birkhoff 1913) the number of the periodic orbits is 2ℓ with an integer ℓ, and in the case of the standard map (Chirikov 1979) ℓ is believed to be one. We do not know the number of non-dominant orbits.

3.3 Periodic orbits and the structure on the Poincaré section

In the present subsection, we study how the dominant periodic orbits are related to the structures on the Poincaré section.

Because of the reversal of the bifurcation at $a = a_{1/3}$, we observe different movements of periodic orbits for two cases: $da > 0$ for $a > a_{1/3}$, and $da < 0$ for $a < a_{1/3}$. In the latter case, there is a nearly periodic change of the Poincaré section, and one cycle in this change is considered to starts from the bifurcation with $\nu_\infty = (n-2)/n$ and ends in the bifurcation with $\nu_\infty = \{(n+1)-2\}/(n+1)$. The change in the former case is basically similar to the one cycle in the latter case (Note that for $a > a_{1/3}$ only $\nu_\infty = 1/3$ has the form $\nu_\infty = (n-2)/n$). Hence, we propose the scenario for the latter case only. The following scenario is based on the observation of the cycles starting, respectively, at $\nu_\infty = 2/4, 3/5, 4/6, 5/7$, and $6/8$.

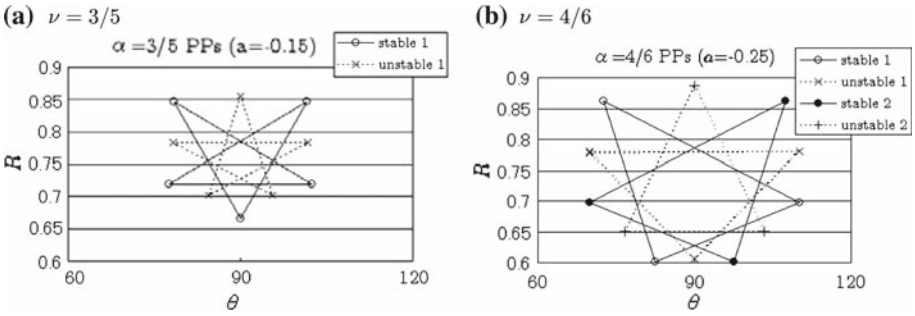

Fig. 7 Periodic orbits for $v_\infty = (n-2)/n$ with (**a**) $n = 5$ and (**b**) $n = 6$. These show the numbers of orbits are 2 for odd n and 4 for even n. We connect the periodic points which belong to the same orbit

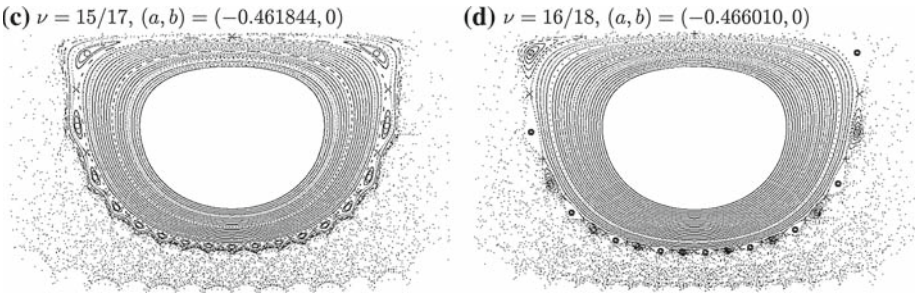

Fig. 8 Periodic orbits for $v_\infty = (n-2)/n$ with (**a**) $n = 17$ and $n = 18$. For each orbit, its orbital points are plotted by different symbols: single and double circles (stable orbits), multiplicative and additive symbols (unstable orbits). Two symbols appear for odd case ($n = 17$), whereas four symbols do for even case ($n = 18$). The background dots shows the Poincaré map of segments of several lines running from $\boldsymbol{P}_0$

In Fig. 9, we describe the result of numerical integrations for mass ratios $-0.150 \geq a \geq -0.250$. We use two expressions for the structure of the Poincaré section: (i) the distribution of triple collision curves, and (ii) the partitioning according to the sets defined in Eq. 6. As seen from panels (a) and (b) of Fig. 9, two expressions extract different aspects of the structure. In panel (a), four black regions around the Schubart region are stability regions of periodic orbits, whereas in panel (b), these regions cannot be seen. In expression (ii), regions from $[\![S_1]\!]$ through $[\![S_{14}]\!]$ are represented by their suffixes and with different colours; primed numbers such as $9'$, $9''$ and so on are used, if such a region $[\![S_9]\!]$ has more than one branches. The dark green region in the center of panels is the Schubart region and the black ones along the θ-axis is scallops (immediate escape regions). Periodic points are marked with circles. Several curves in the Schubart region represent the orbits close to the periodic orbits; the shape of these curves reflect the stability of the periodic orbits.

Let us show our scenario by describing events on the Poincaré section with the decrease of a. The bifurcated periodic points with $v_\infty = (n-2)/n$ ($n \geq 4$) recede from $\boldsymbol{P}_0$. As the distances become larger, the stability regions (hereafter called *islands*) around the periodic points more strongly influence the shape of the Schubart region. An example in this stage for odd n cases ($n = 5$) are shown in panels (a) $a = -0.150$ and (b) $a = -0.160$ in Fig. 9. The points s_i and u_i ($i = 1, \ldots, 5$) are the orbital points of stable and unstable periodic orbits with rotation number $v_\infty = 3/5$. Five triangular islands are not separated from the central

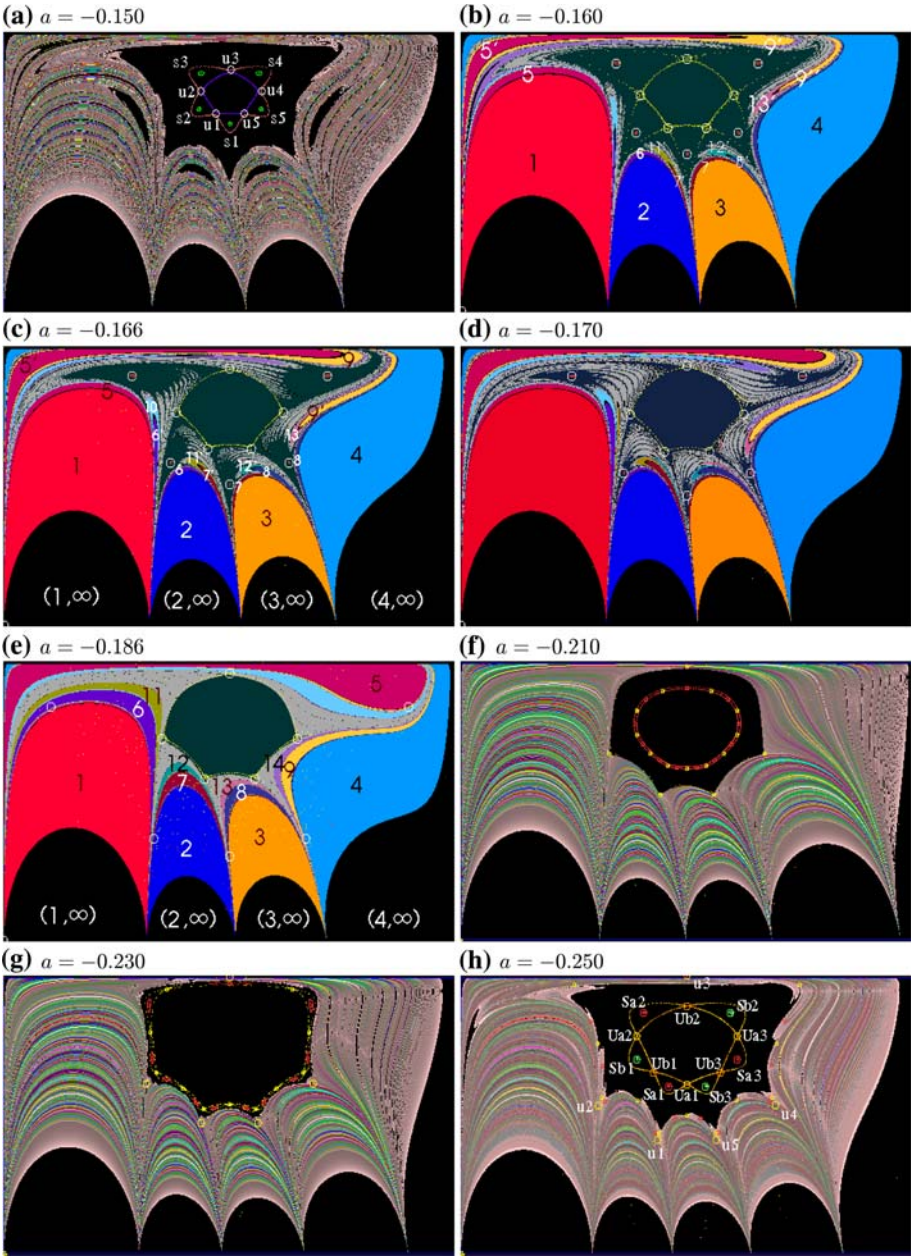

Fig. 9 Periodic orbits and the structure of the Poincaré section. The enlargement of islands as a decreases in panels (**a**) and (**b**). Growing germs along the pentagonal Schubart region in (**c**). Germs splitting the Schubart region into the new Schubart region and islands in (**d**). Invisible stability regions of the bifurcated orbits (their orbital points are circled) in (**e**). The existence of non-dominant periodic orbits with $\nu_\infty = 7/11$ in (**f**) and (**g**). The cohabitation of periodic orbits with $\nu_\infty = 3/5$ and $\nu_\infty = 2/3$

pentagonal region, and therefore, the shape of the Schubart region changes from polygonal to polygramic as the islands become larger. The intrusion of germs cuts islands from the Schubart region; the shape of the Schubart region returns to polygonal but the number of vertices increases. Panels (b) $a = -0.160$ and (c) $a = -0.166$ imply that the periodic points with $\nu_\infty = (n-2)/n$ $(n = 5)$ get out of the Schubart region at a certain mass ratio in the interval $-0.160 \geq a \geq -0.166$. As a further decreases, the stable periodic points sink into the gaps between arches and their islands shrink, whereas the unstable periodic points stay around the vertices of the Schubart region. The comparison of panels (d) $a = -0.170$ and (e) $a = -0.186$ shows this tendency. In the latter panel, the stability region of the periodic points (their positions are circled) is no longer visible. We shall show in the next paragraph more detailed numerical evidence which supports the arrival of these points at the θ-axis. Germs grow to follow the periodic points. This behaviour of germs reconstructs arches: for example, the second arch consists of regions $[[S_2]]$, $[[S_6]]$, etc. in panel (b) $a = -0.160$, whereas of $[[S_2]]$, $[[S_7]]$, $[[S_{12}]]$, etc. in panel (e) $a = -0.186$. The Schubart region has $(21)^n$ with infinite n, whereas surrounding arches also have $(21)^n$ but with a finite n. There are similar relations between the stability region of the bifurcated orbits and germs surrounding it.

According to Paper I, the arch reconstruction and the construction of a new arch is completed at the totally degenerated case $a \fallingdotseq -0.208$, which is near the case shown in panel (f) $a = -0.210$. Interestingly, mass parameters at which periodic orbits bifurcate are far from those of total degeneracies. Two panels (f) and (g) $a = -0.230$ show that non-dominant periodic orbits have limited influence on the Poincaré section: $\nu_\infty = 7/11$ in the case of these panels. The latter panel captures a scene that the stability regions of these orbits slightly distort the edges of the Schubart region. The other non-dominant orbits between the bifurcations for $\nu_\infty = 3/5$ and $\nu_\infty = 4/6$ have negligible influence. In a further smaller a, panel (h) $a = -0.2500$, dominant periodic orbits with the next rotation number $\nu_\infty = 4/6$ have bifurcated, which is an example for even n case. There are no difference between odd n cases and even n cases in the effect of the orbits on the Poincaré section; in even n cases, the period of orbits is $n/2$, whereas the number of orbits is four. The positions of periodic points are labeled in panel (h): u_i for the unstable orbit with $\nu_\infty = 3/5$, Sa_i and Sb_i for stable orbits with $\nu_\infty = 4/6$, and Ua_i and Ub_i for unstable orbits with $\nu_\infty = 4/6$. This panel shows the cohabitation of dominant unstable periodic orbits with different rotation numbers.

3.4 Fate of bifurcated periodic orbits

Where do bifurcated periodic points finally go as a decreases? Although the unstable ones are uncertain, we conjecture that the stable ones reach θ-axis and coincide with some foot-points at a totally degenerated case. In the following paragraphs, we show numerical collateral evidence for the arrival of stable points on the θ-axis, discuss the coincidence between this arrival and the total degeneracy, and again show numerical results which suggest how periodic orbits changes their shape as their orbital points approach the θ-axis.

Figure 10a shows the dependence of R on a for one orbital point of one of two stable periodic orbits with $\nu_\infty = 2/4$. As a decreases, R monotonically decreases. This figure indicates that this periodic point approach to $R = 0$ at least down to $R = 0.0579$ (at $a = 0.022$). We do not calculate this periodic point below $a = 0.022$, since it is extremely hard.

Figure 10b shows the dependence of dR/da on a, which is derived from the data plotted in Fig. 10a. Since dR/da takes a non-negligible non-zero value at $a = 0.022$, it is expected that, R further decreases and reaches zero at some smaller value of a than 0.022. The derivative dR/da is approximately linear in the range $a < 0.0275$. Therefore, the a versus R curve

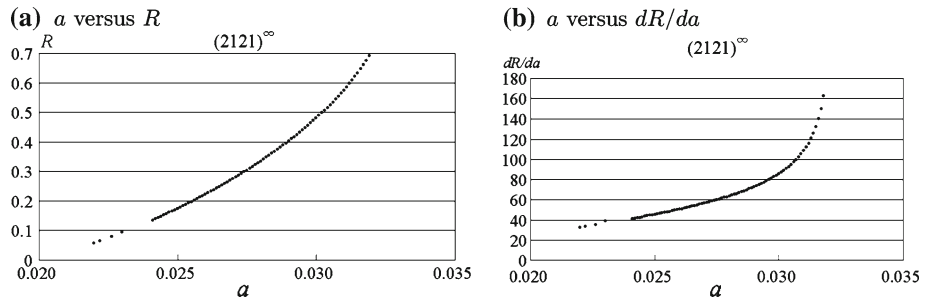

Fig. 10 A family with $v_\infty = 2/4$ bifurcated from the Schubart orbit: the dependence of R and dR/da on a is plotted for a selected orbital point

well fits to a quadratic function in this range. Solving the fitted quadratic function for a, we have $a = 0.01965$ at $R = 0$. This is near the value of a totally degenerated case, $a = 0.0198$.

There are three possibilities of the fate of stable periodic points: (a) stay at some $R > 0$ region, (b) reach $R = 0$, and (c) merge and bi-annihilate with unstable periodic points. Although we have conjectured that the case (b) occurs, we here consider the other possibilities. The a versus dR/da curve shown in the previous paragraph rather supports the case (b) than the case (a). The case (c) is also considered to be less possible, since stable periodic points reach very close to the $R = 0$, whereas unstable periodic points seem to stay around the Schubart region. We next mention why we consider that the case (b) occurs only in total degenerate cases. The discussion below is based on the theoretical results for *fictitious orbits* (intuitively, limit orbits with initial condition $R \to 0$) in (McGehee 1974). In order to occur the case (b), an orbit has to approach some fictitious orbit with keeping its periodicity. It must be impossible except totally degenerated cases, since all fictitious orbits are (corresponding to) past or future escaping orbits in non-degenerate cases. In totally degenerated cases, a fictitious orbit which intersects with foot-points makes a close curve together with the homothetic orbit. We consider that periodic orbits approach to this close curve, and therefore, that their orbital points approach foot-points.

A fictitious orbit intersects with foot-points in totally degenerated cases starts at and ends with triple collisions. Figure 11 suggests, how a periodic orbit approaches such a triple collision orbit. The geometrical scale of the triple system is roughly constant in the Schubart orbit as is shown in the panel (a) ($a = 0.030$). In a bifurcated orbit, there are durations in which this scale becomes small as is shown in the panel (b) ($a = 0.030$). This scale becomes further smaller in these duration as a decreases as is shown in the panel (c) ($a = 0.024$). Note that, although the orbit seems not to be periodic in the panel (c), this is due to the error of initial values (in an order of 10^{-12}). The periodic orbit shown in panels (b) and (c) is expected to approach the fictitious triple collision orbit with the symbol sequence 210.

3.5 Non-Schubart periodic orbits

We have ignored four black regions surrounding the Schubart region in Fig. 9a $a = -0.15$. These are the stability regions of two 2-periodic orbits. In these stability regions, the symbol sequence is $(21121)^\infty$, which is different from that of the Schubart region. Figure 12 shows the family to which one of these orbits belongs as a curve of a versus R. The tangential line of the curve seems to be perpendicular to the a-axis at the right terminal ($a \fallingdotseq 0.021$). Therefore, it is expected that, a tangent bifurcation occurs near $a = 0.021$ and yield this family.

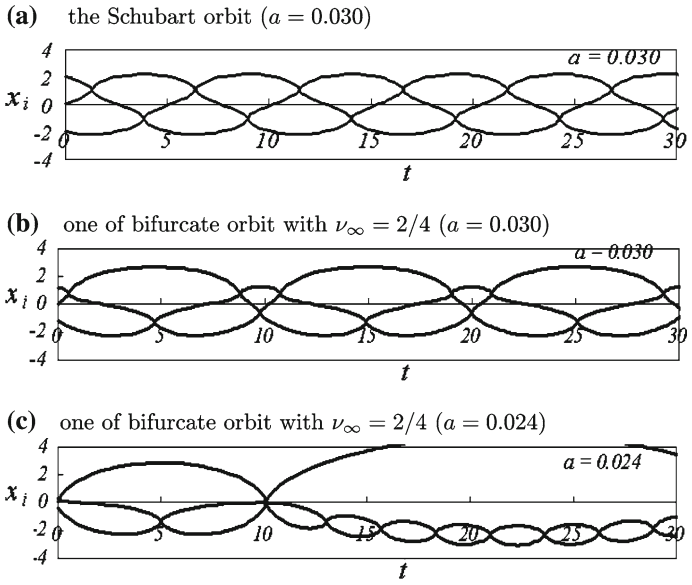

Fig. 11 Time dependence of orbits in a family shown in Fig. 10: the vertical axis shows the position x_i of each particle ($i = 1, 0, 2$)

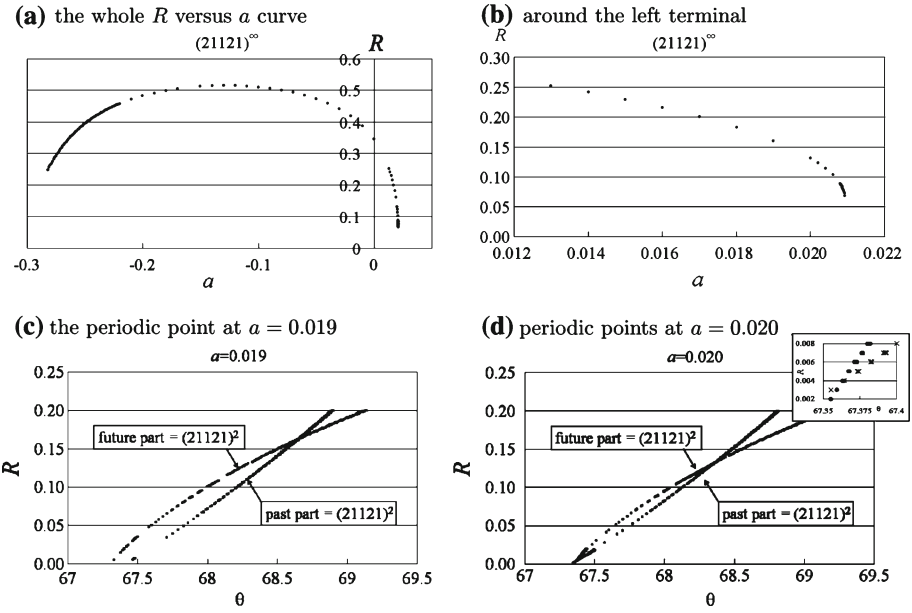

Fig. 12 A family with symbol sequence $(21121)^\infty$: an example of periodic orbits not bifurcated from the Schubart orbit. The panels (**a**) and (**b**) are plotted in a similar manner to Fig. 10a. The panels (**c**) and (**d**) show the intersection of two regions in the Poincaré section: the future part of the symbol sequence is $(21121)^2$ in one region and the past part is $(21121)^2$ in the other region

In order to confirm that, this tangent bifurcation occurs, we have to find some periodic orbit in another branch of this family. We use a method (Tanikawa and Mikkola 2000b) based on the distribution of symbol sequences on Π to find such an orbit. If an orbit is periodic, both of the future part and the past part of its symbol sequence has a form w^∞ with a finite word w. Therefore, regions where its orbital points can exist are obtained as intersections of such two region that the past part of symbol sequence is w and the future part is arbitrary in one region and it is opposite in the other region (although we omit the discussion here, the periodic points actually exists in the intersections). This is the idea of this method. Panels (c) and (d) in Fig. 12 show the intersection of these region for the case $w = 21,121$. These regions are narrow and look like almost curve. One region intersects with the other region twice at $a = 0.020$ (Fig. 12d). This two intersection indicates that there is another undetected periodic point and hence a tangent bifurcation occurs: the intersection at the lower value of R corresponds to the undetected periodic point. This periodic point is expected to reach $R = 0$ and to disappear at some a between 0.019 and 0.020, since the lower intersection disappears at $a = 0.019$ (Fig. 12c).

4 Summary

We have studied the movement of periodic points bifurcated from the fixed point (the Schubart orbit) and their influence on the structure of the Poincaré section in symmetric mass configurations. The following is the summary of the present paper.

- The periodic orbits whose rotation number has a form $(n-2)/n$ with integer $n \geq 3$ are influential on the structure of the Poincaré section. As for these orbits, one pair of orbits with period n bifurcate if n is odd, whereas two pairs of orbits with period $n/2$ bifurcate if n is even.
- There is a value $a = a_{1/3}$ where the rotation number is 1/3 at the fixed point. Whether a increases or decreases from $a_{1/3}$, periodic orbits bifurcate from the Schubart orbit one after another. This fact derives that bifurcated orbits from the Schubart orbit does not exist at $a = a_{1/3}$.
- While periodic points are inside the Schubart region, germs grow along their separatrices in a polygramic shape. After these periodic points get out of the Schubart region, germs grow along their separatrices in a polygonal shape. Corresponding to this, the Schubart region changes their shape from a polygramic one to a polygonal one.
- Stable periodic points leave the fixed point quickly as a decreases. They collect germs and sink toward the θ-axis. This collection of germs results in re-composition of arches. On the other hand, unstable periodic points stay around the vertices of the Schubart region.

Acknowledgements Our paper is improved to the current form according to advices of the reviewers. We would like to express to them our gratitude for the advices.

References

Birkhoff, G.D.: Proof of Poincaré's geometric theorem. Trans. Am. Math. Soc. **14**, 14–22 (1913)
Chirikov, B.V.: A universal instability of many-dimensional oscillator systems. Phys. Rep. **52**, 263–379 (1979)
Contopoulos, G.: Order and Chaos in dynamical astronomy. pp. 139–143. Springer, Berlin (2002)
Hénon, M.: Numerical exploration of the restricted problem. VI. Hill's case: Non-periodic orbits. Astron. Astrophys. **9**, 24–36 (1970)

Hietarinta, J., Mikkola, S.: Chaos in the one-dimensional gravitational three-body problem. CHAOS **3**, 183–203 (1993)
McGehee, R.: Triple collision in the collinear three-body problem. Inventiones Mathematicae **27**, 191–227 (1974)
Mikkola, S., Hietarinta, J.: A numerical investigation of the one-dimensional Newtonian three-body problem I. Celest. Mech. Dyn. Astron. **46**, 1–18 (1989)
Mikkola, S., Hietarinta, J.: A numerical investigation of the one-dimensional Newtonian three-body problem III. Celest. Mech. Dyn. Astron. **51**, 379–394 (1991)
Moser, J.: Stability of the asteroids. Astron. J. **63**, 439–443 (1958)
Orlov, V. V., Petrova, A. V., Tanikawa, K., Saito, M. M., Martynova, A. I.: The rectilinear three-body problem. Celest. Mech. Dyn. Astron. **100**, 93–120 (2008)
Saito, M.M., Tanikawa, K.: Collinear three-body problem with non-equal masses by symbolic dynamics. ASP Conf. Ser. **316**, 63–69 (2004)
Saito, M.M., Tanikawa, K.: The rectilinar three-body problem using symbol sequence I. Role of triple collision. Celest. Mech. Dyn. Astron. **98**, 95–120 (2007)
Sano, M.: The classical Coulomb three-body problem in the collinear eZe configuration. J. Phys. A Math. Gen. **37**, 803–822 (2004)
Schubart, J.: Losungen im Dreikörper problem. Astronomische Nachrichten **283**, 17–22 (1956)
Tanikawa, K., Mikkola, J.: Triple collisions in the one-dimensional three-body problem. Celest. Mech. Dyn. Astron. **76**, 23–34 (2000)
Tanikawa, K., Mikkola, J.: One-dimensional three-body problem via symbolic dynamics. CHAOS **10**, 649–657 (2000)